Process Intensification of CO_2 Capture by Low-Aqueous Solvent

Gyoung G. Jang, Joshua A. Thompson, Xin Sun, and Costas Tsouris*

Manufacturing Science Division, Oak Ridge National Laboratory, Oak Ridge, TN 37831

*Corresponding author: tsourisc@ornl.gov

Submitted to:
Chemical Engineering Journal

April 2021

Abstract

Low-energy solvent-based CO_2 absorption processes have drawn attention as a next-generation post-combustion CO_2 capture technology to reduce CO_2 emissions from fossil fuel– or biomass-fired power generation and industrial flue gas streams. A low-aqueous (or water-lean) solvent process may substantially reduce the thermal energy consumption for solvent regeneration. Low-aqueous solvent–based processes are thermally sensitive, requiring a delicate temperature control within the absorber because of the fast exothermic amine-CO_2 reaction and low heat capacity organic diluent. This reaction may result in heat accumulation in a packed absorption column and undesirable CO_2 desorption occurring as the solvent moves through the column, reducing the solvent's CO_2 capture efficiency if its temperature is not controlled. Using a 3D printed intensified packing device, enhanced heat and mass transfer were demonstrated in an amine-CO_2 scrubbing process using low-aqueous solvent. The multifunctional intensified device facilitates contact of the reactive solvent and gas phases in a single stage and heat removal by a cooling fluid flowing through channels in the interior of the corrugated plates of the device. These functionalities led to effective thermal management along the column via intrastage cooling and significant improvement in CO_2 uptake under a wide range of operating conditions. Intrastage cooling effectively reduced the solvent average temperature along the column by ~10°C and, as a result, the solvent's capture efficiency improved by up to 25%.

Keywords: CO_2 capture; low-aqueous solvent, intensified packing, process intensification, additive manufacturing

I. Introduction

Carbon capture and storage is an effective method of reducing greenhouse gas emissions and the associated global warming effects. During the past two decades, a variety of CO_2 capture technologies—including chemical solvent absorption, solid adsorption, biological fixation, membrane separation, photocatalytic conversion, and gas-hydrate–based separation—have been investigated [1−6]. Among these techniques, solvent-based CO_2 absorption is the most mature technology for CO_2-rich gases, such as the emissions from fossil fuel– and biomass-fired power plants and industrial flue gas streams [7]. Solvent-based CO_2 absorption, however, is also considered one of the most energy-intensive CO_2 capture methods because solvent regeneration requires substantial thermal energy [7− 9], which is the largest contributor to the process operating cost. A traditional amine-based CO_2 capture solvent (e.g., 30 wt % monoethanolamine [MEA] in water) requires relatively large amounts of thermal energy for heating the solvent during the regeneration process. For example, the reboiler heat duty of aqueous MEA has been estimated to be 3.1–3.75 MJ/kg CO_2 [10,11].

Toward the reduction of the operating cost, many solvent mixtures such as amine/ammonia-based solvents, nanofluids, water-lean solvents, and nonaqueous solvents have been studied over the past 20 years [12− 15]. An ideal solvent should have high CO_2 absorption capacity, fast reaction rate, low cost, low corrosivity, high thermal and chemical stability, low vapor pressure, and low regeneration heat duty. There are three main contributors to the regeneration heat (Q_{reg}) needed to release CO_2 bonded with amine molecules: (1) the sensible heat (Q_{sen}) required for the solvent to reach the regeneration temperature (e.g., 105°C–110°C), (2) the heat of vaporization (Q_{vap}) for fractional vaporization of the solvent, and (3) the heat of the amine-CO_2 reaction (ΔH_{abs}):

$$Q_{reg} = Q_{sen} + Q_{vap} + \Delta H_{abs} \quad (1)$$

The sensible heat and the heat of vaporization can be significantly reduced by replacing water with a low–specific heat capacity and low–vapor pressure solvent. The heat of vaporization depends on the amount of water, which is the largest fraction by weight in CO_2-loaded aqueous amine solutions [10, 15−17]. A concentrated aqueous amine solution containing less water and more of a lower–vapor pressure diluent would result in less latent heat of vaporization for the solvent [18]. Several studies have focused on the development of non- or low-aqueous solvents (LASs) to decrease the sensible heat requirement and the heat of reaction [14,15,17,19]. For example, some solvents (e.g., water-lean amine solvent containing N-(2-ethoxyethyl)-3-morpholinopropan-1-amine [2-EEMPA]) result in reboiler duty reduction for regeneration up to 2.0 MJ/kg CO_2, a 55% decrease in duty compared with traditional aqueous solvents [14].

An ideal LAS should have lower sensible heat, improved reaction rate between the amine and CO_2, and lower reaction enthalpy than aqueous MEA [9−11,19]. An example of LAS is N-methylbenzylamine (NMBZA), which is a secondary amine with an aromatic functional group investigated in both hydrophobic and hydrophilic diluent systems with the goal to reduce the amount of water [19]. By using a hydrophobic diluent system, the activation energy of the amine was reduced to 10.37 $kJmol^{-1}$, compared to 22.76 $kJmol^{-1}$ of an aqueous system. The organic carrier has lower specific heat capacity, i.e., C_p = 2.2 $kJkg^{-1}K^{-1}$ at 40°C, and heat of vaporization on a mass basis than aqueous MEA, where water C_p = 4.18 $kJkg^{-1}K^{-1}$ at 40°C. The low amount of water added in the hydrophobic diluent system also acts as an activator, increasing the reaction rate. Finally, another advantage is the lower vapor pressure of the solvent, which reduces the solvent heat of vaporization during regeneration and lowers solvent emissions.

Although LAS has a relatively high reaction rate with CO_2 that is desirable for CO_2 absorption, the solvent still requires delicate thermal control because of the heat generated during the reaction. In general, CO_2-amine absorption is an exothermic reaction and releases significant heat (e.g., 80–100 kJ/mol for 30 wt % aqueous MEA solvent at 40°C) [20]. The heat released by this exothermic reaction may accumulate in the absorption column, and the bulge temperature along the column can exceed 70°C [21,22]. Approximately 60% of the absorbed CO_2 desorbs at 90°C, and higher temperatures (100°C or greater) are used for CO_2 desorption and solvent regeneration [23]. The temperature-dependent desorption behavior is favorable for regenerating the solvent; however, it may have a negative effect on the CO_2 capture efficiency when the heat of reaction accumulates in the column [22−25]. To reduce effects from temperature increase within the absorber, effective interstage cooling using external heat exchangers may be required in a full-scale CO_2 absorption column, increasing the capital and operating costs [24].

Recently, we developed an additively manufactured packing device capable of removing excess heat from a gas-liquid reactive system via intrastage cooling as a good example of *modular chemical process intensification* and demonstrated enhanced mass and heat transfer during CO_2 absorption, resulting in improved CO_2 capture efficiency [25−27]. This device is referred to here as intensified device because of its dual functionality, i.e., enhancing mass transfer, like conventional structured packing elements do, while also working as heat exchanger. A traditional interstage heat exchange system requires pumping the solvent outside the column, which would increase complexity and cost. The combination of two different unit operations, e.g., heat exchange and mass transfer into a single device can dramatically improve energy and process efficiency and help achieve size reduction and environmental impact mitigation [28], which are process-intensification objectives. Because most structured packing elements consist

of corrugated plates [29], traditional heat-exchanger–reactor manufacturing concepts are difficult to adopt toward achieving process intensification. In this study, it is shown that additive manufacturing, also known as 3D printing, can be used to overcome the barriers of traditional manufacturing techniques with complicated designs and achieve multifunctionality, leading to process intensification. The intensified device integrates heat transfer from reactive fluids to a cooling fluid flowing within channels in the interior of the corrugated plates of the packing element and mass transfer between the gas and solvent phases flowing between corrugated plates. These functions of the intensified device are shown in Figure 1.

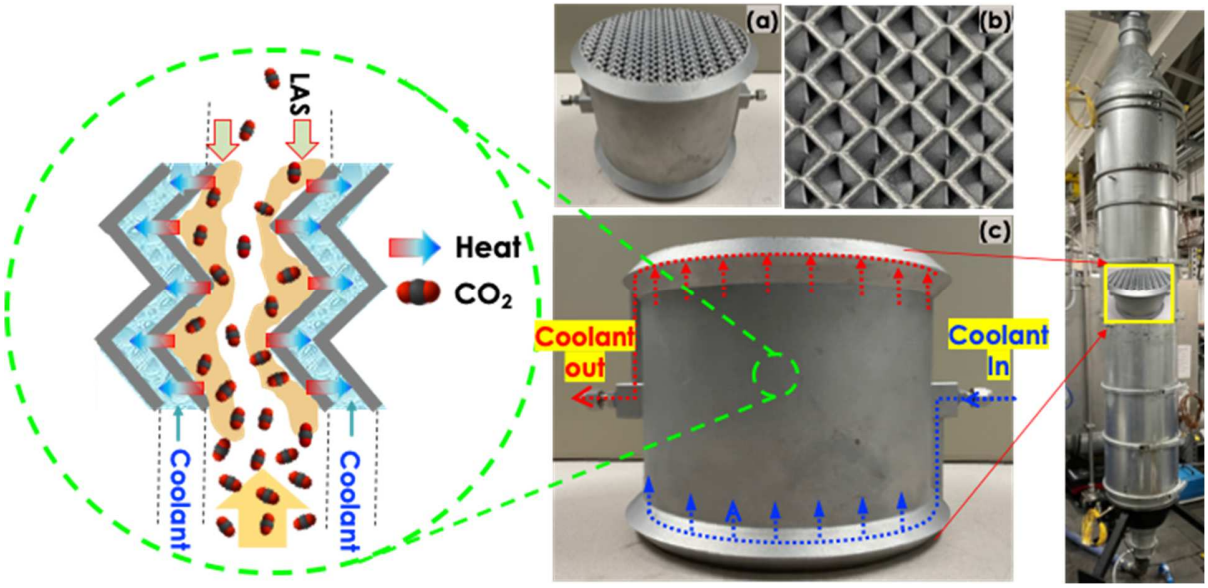

Figure 1. (a) Additively manufactured intensified reactive packing device for CO_2 amine solvent absorption and heat exchange. (b) Top view of corrugated channels for counter current flue-gas scrubbing by the solvent. (c) Front view of intensified device with heat and mass transfer functions.

The coolant fluid flows around the perimeter of the device and enters spaces within the corrugated plates (baffles). Inside those spaces, the coolant channels run parallel to the corrugation angle so that coolant flows counter-currently with the liquid solvent and co-currently with the gas. Reaction between CO_2 and the solvent occurs within the liquid film on the surface

of the corrugated channels, where heat is also released because of the exothermic reaction. The heat is then transferred through the wall of corrugated plates and removed by the coolant flowing through the channels. The inlet and outlet for the coolant are positioned on the sides of the device. The intensified device can be positioned inside the absorption column, preferably near the point where a bulge temperature is expected, to eliminate the need for traditional external heat exchangers, thus reducing complexity and capital and operating costs.

The additively manufactured structured packing is also compatible with commercially available structured packing elements that are widely used in gas–liquid or liquid–liquid systems. This alternative intrastage cooling system has been shown to effectively enhance heat transfer from the solvent to the coolant and CO_2 uptake by aqueous MEA under a range of operating conditions [27]. Table 1 compares the functionality of the intensified device with other intensification techniques for CO_2 capture discussed recently in the literature.

In the present study, we employ an additively manufactured intrastage cooling device that has been developed in our laboratories to overcome a major barrier of a LAS system for CO_2 capture, which is the sensitivity of the solvent to temperature increases due to its exothermic reaction with CO_2. We report results of process intensification via intrastage cooling of the reactive system using the intensified packing element to achieve mass and heat transfer enhancement for a range of operating parameters, including gas and solvent flowrates and solvent feed temperature. Additionally, an equilibrium model was developed to predict the temperature and CO_2 profiles along the column, and simulation results are compared with experimental data.

Table 1. Process intensification techniques in CO_2 capture

Technique	Source/Solvent	Intensification Parameter	Consideration	Testing Scale (m)	Reference
Rotating Packed Bed/Spiral Contactor	Natural gas (4% CO_2) / 30% MEA	Mass transfer; Controlling liquid film thickness (e.g., 2.7× higher mass transfer) Absorber and stripper size reduction (e.g., 1/3 volume reduction)	Device Scalability Thermal control Adaptability for the existing facility	0.398 m (ID) × 0.025 m (height)	[30]
	Natural gas (2–6% CO_2) /potassium sarcosine			0.05m (ID) × 0.05m (height)	[31]
	Flue gas (10% CO_2) /Diethanolamine			0.9 m (OD) × 0.004m (height)	[32]
Microreactor	Flue gas (10% CO_2) /Diethanolamine	Mass transfer; Controlling liquid film thickness by microchannels Micro hydraulic diameter (e.g., 1~3 order of magnitude enhanced mass transfer)	Large scale channel geometries Thermal control Adaptability for the existing facility	0.455 m (length) × 0.004m (hydraulic diameter)	[33]
Membrane reactor	Flue gas (11.6% CO_2) /Membrane	Gas separation (e.g., diffusivity) High CO_2 /N_2 selectivity	Large scale, High permeance, Membrane cost, Reliability	Lab scale	[34]
Thermal integration (Interstage)		Heat integration strategy for various systems (Hollow fiber sorbent, packing bed solid sorbent, membrane, solvent absorption	Interstage heat exchange system Complication		[35]
Intrastage intensified device	Flue gas (~14% CO_2) /30% MEA & LAS	Heat & Mass transfer Absorber and stripper size reduction/High adaptability to the existing absorption column		0.203 m (OD) × 0.146 m (height)	[26] & this study

II. Experimental Section

Materials: A volume of 35 gal of LAS provided by RTI International (USA) was used in this work. The solvent consists of a diamine, organic diluent, and water. The boiling point of this solvent is 185°C–243°C, which is higher than that of the aqueous MEA. The viscosity and density of the solvent at 20°C are 4.5 cP and 1.035 kg/L, respectively, which are comparable to those of aqueous MEA at the same temperature.

Intensified packing device: The intensified packing device was designed at Oak Ridge National Laboratory's Manufacturing Demonstration Facility and manufactured by Volunteer Aerospace LLC (Knoxville, Tennessee). The device incorporates separate channels for reaction and heat exchange into the same device where the 3D printed structured packing shown in Figure 1 enables coolant channels to be integrated into a packing element [25–27]. Previous studies have characterized the hydrodynamic and wettability characteristics of the printed packing, and no loss in hydrodynamic performance is reported relative to commercial packing [26]. The final intensified device prototype measures 20.3 cm in diameter, 14.6 cm in height, and the total volume of the internal coolant channels is 600 mL. Aluminum was used to fabricate the intensified packing device because of its printability and high thermal conductivity.

Absorption column: An absorption column of 2.06-m height and 0.2-m diameter was operated in a counter-current mode, where LAS was fed to the column from the top and CO_2-rich flue gas was inserted at the bottom [27]. The column consisted of the intensified packing device and seven stainless-steel Mellapak 250Y commercial packing elements (CPEs) acquired from Sulzer (Winterthur, Switzerland). The column was double walled to reduce heat exchange with the room atmosphere and achieve near adiabatic conditions. A thermally insulating polymer tube

was used for the main column and an outer metal shell surrounding the inner column was used for support and to avoid heat losses (Figure 2).

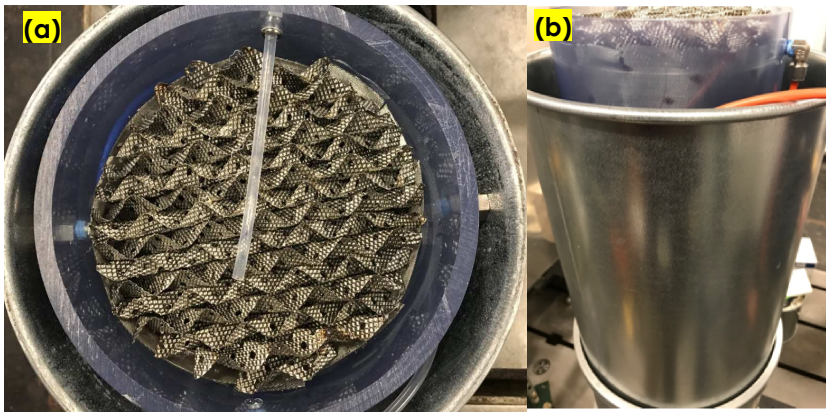

Figure 2. Structure of column with stainless-steel Mellapak 250Y commercial packing elements: a) top view, b) side view. The inner tube was made from high-density polyethylene.

The intensified device was placed on the top half of the column in the arrangement outlined in Figure 3, with four CPEs located below and three CPEs located above the intensified device. The total bed height occupied by packing elements, including the intensified device, was 1.58 m. The simulated CO_2-rich flue gas was a mixture of air and pure CO_2 at various concentrations. A blower supplied the air at specified flow rates, and the CO_2 was sourced from pressurized gas cylinders. The CO_2 flow rate was set by a Teledyne THCD-101 (Thousand Oaks, California) mass flow controller. The separate streams of air and CO_2 were then mixed and proceeded to enter the absorption column from the bottom. A complete schematic of this experimental system is shown in Figure 3.

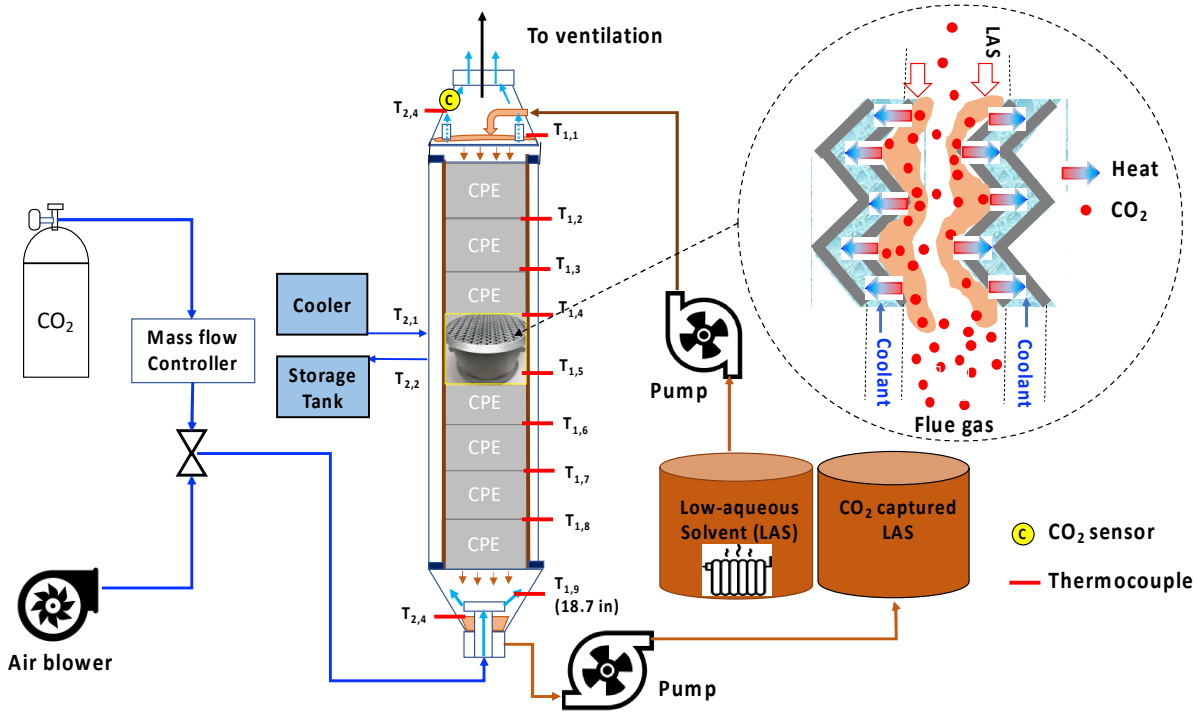

Figure 3. Schematic of Oak Ridge National Laboratory testing facility and CO_2 absorption column.

CO_2 measurements: CO_2 capture efficiency measurements were obtained using a CO_2 meter manufactured by CO_2 Meter (Ormond Beach, Florida). The exit concentration of CO_2 was measured at the top of the column, the exit point for the gas stream. The nominal initial concentration was determined by the mass flow controller and blower settings; however, it was verified by allowing the gas stream to continue flowing up the column after the solvent stream was cut off and then recording the resulting concentration. The CO_2 capture efficiency was calculated as

$$Capture\ efficiency\ (\%) = \frac{CO_2\ (\%)\ in\ Feed - CO_2\ (\%)\ in\ Output}{CO_2\ (\%)\ in\ Feed} \times 100 \qquad (2)$$

Thirteen liquid temperature readings along the height of the column were obtained using type K thermocouples. A time-dependent temperature profile was automatically generated by PicoTech (Cambridgeshire, UK) temperature data recording software at a specified sampling rate of 1/s.

Geometric temperature profiles were generated by taking the average of the time-dependent temperature profile over 1 min after steady state was reached.

Characterization of solvent: The water amount in the LAS was determined by Karl Fischer titration. A CM140 Total Inorganic Carbon Analyzer comprising an Acidification Module CM5330 and a CO_2 Coulometer CM5017 was used to measure the total inorganic carbon in aqueous and organic solutions. The Acidification Module used air as the carrier gas, set to 100 mL/min, which was scrubbed with 45% KOH solution to remove CO_2 from the air. 5 mL of 2 M HCl was added to 0.1–1 mL of sample solution to release CO_2. A scrubber containing 50% KI solution was used to remove H_2S, SO_x, and/or halogens from the resulting mixture of gases that might result from acidification of the samples. Commercially available cathode and anode solutions and KI were used for the CO_2 Coulometer cell.

CO_2 absorption experiments: A series of experiments were carried out to provide a better understanding of the influence of feed temperature, L/G ratio (i.e., solvent over gas flow rate ratio), cooling, and regeneration on CO_2 capture performance (Table 2). The feed gas was a simulated flue gas with 13–14% CO_2). The feed solution temperatures ranged between 40 and 60°C. The influence of the operating parameters (mainly L/G ratio) was investigated at a fixed temperature (40°C). Each run requires 40–50 L of solvent (LAS). LAS was regenerated at ~105°C for 30 min. Before and after regeneration, samples of CO_2 rich and lean LAS solvents were collected to measure the content of CO_2 and water. After the second regeneration, deionized water was added to investigate the influence of water concentration. Time-dependent temperature profiles along the column before and after cooling were recorded to identify the temperature bulge.

III. Modeling Framework

A simplified equilibrium-stage model framework was used to compare absorption modeling results with the observed column temperature profile for the LAS and the outlet CO_2 concentration from the experiments. The solubility of CO_2 was determined by a vapor-liquid equilibrium model using a semi-empirical Virial expansion, adopted from Chen and Rochelle [36], to determine the equilibrium partial pressure of CO_2 based on the loading in the solvent:

$$y^*_{CO_2} P = P^*_{CO_2} = \exp\left(\sum_{j=0} \left(A_j \right.\right. \tag{3}$$

where $y^*_{CO_2}$ and $P^*_{CO_2}$ are the equilibrium mole fraction in the vapor phase and the partial pressure for CO_2 that is in equilibrium with the CO_2 loading in the solvent, α (mol CO_2/mol amine), P is the total system pressure, A_j and B_j are Virial expansion constants, and j is the Virial expansion term starting at zero. Water and amine in the solvent were also considered in the absorption modeling, and the ideal Raoult's law was used to determine the equilibrium partial pressure for these components:

$$y^*_i P = P^*_i \tag{4}$$

where x_i is the mole fraction of component i, water or amine, in the solvent and P_i^{sat} is the vapor pressure of component i. The solubility of O_2 and N_2 in the LAS and the vaporization of the organic diluent were assumed negligible. Therefore, the component mass balances for each stage assume no transfer of O_2 and N_2 from the gas to the solvent and no transfer of the organic diluent from the solvent to the gas.

Figure 4 shows an illustration of the equilibrium-stage model used for the absorption simulations. Because of the absorption column used in the experiments having a fixed number of

packing elements, a fixed number of stages equal to the number of packing elements in the experiment, $N_z = 8$, was used in the absorption model.

The overall mass balance in each stage, z, can be written as

$$L_{z+1} - L_z + V_{z-1} - V_z = 0 \tag{5}$$

where L and V are the total liquid and vapor molar flow rates, respectively. The component material balances are

$$x_{i,z+1}L_{z+1} - x_{i,z}L_z + y_{i,z-1}V_{z-1} - y_{i,z}V_z = 0 \tag{6}$$

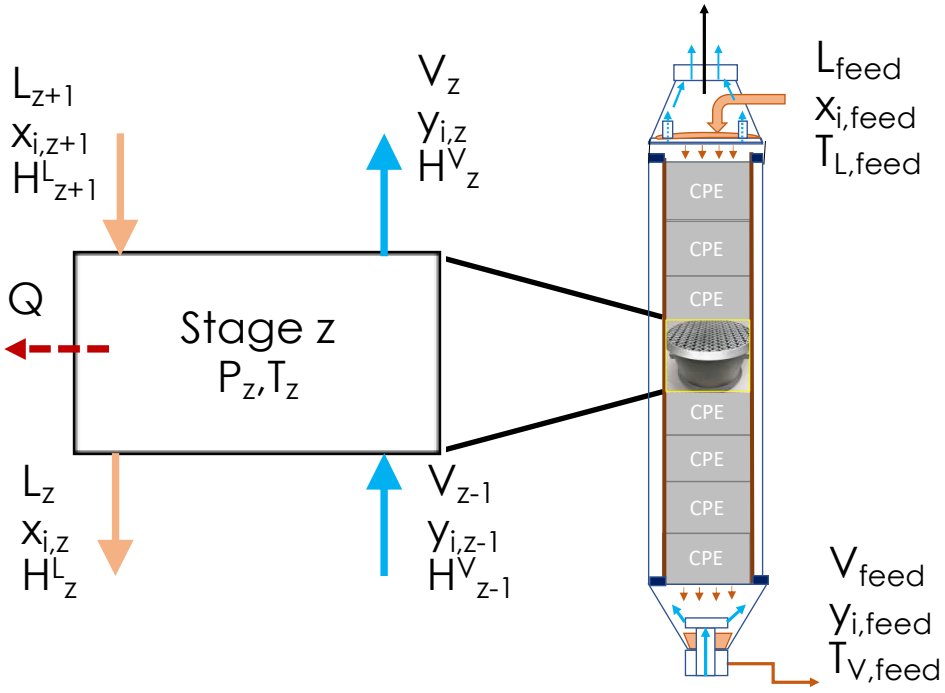

Figure 4. Schematic of equilibrium-stage absorption model with intrastage cooling.

The energy balance is determined by

$$h_{L,z+1}L_{z+1} - h_{L,z}L_z + h_{V,z-1}V_{z-1} - h_{V,z}V_z + \Delta H_R - \Delta H_{vap,H_2O} - \Delta H_{vap,am} - Q = 0 \tag{7}$$

where h_L and h_V are the enthalpies of the vapor and liquid, respectively, ΔH_R is the heat of reaction generated at each stage by CO_2 absorption into the solvent from the vapor, $\Delta H_{vap,i}$ is the heat of vaporization generated by water and amine at each stage, and Q is the heat loss during

cooling experiments at the stage containing the additively manufactured structured packing. The heat of reaction is the summation of the CO_2 dissolution into the solvent and reaction with the amine [37]:

$$\Delta H_R = \Delta H_{abs} + \Delta H_{diss} \tag{8}$$

where ΔH_{abs} is the heat of absorption, and ΔH_{diss} is the heat of dissolution for CO_2. The heat of absorption for CO_2, which may be assumed as the heat generated by the reaction with amine, was determined using the Gibbs-Helmholtz equation for the semi-empirical Virial solubility model:

$$\Delta H_{abs} = -R \frac{d \ln P}{d\, {}^1\!/_T} = -R \sum_{j=0} (B_j)\, \alpha^j \tag{9}$$

where R is the ideal gas constant, 8.314 J/mol/K. The heat of dissolution was assumed to be equivalent to CO_2 dissolution in water [38]:

$$\Delta H_{diss} = R(-5284.795 + 95.04081T - 0.32395T^2 + 0.000152T^3) \tag{10}$$

where the constants are derived from Edwards et al. [38]. Because water was used as the coolant in the cooling experiments, the heat loss may be determined by

$$Q = m_{H_2O} \int Cp\, dT \tag{11}$$

where m_{H_2O} is the mass flow rate of water, and C_p is the heat capacity.

The nonideal behavior in absorption columns was approximated by assuming a stage efficiency. To simplify the model, a universal stage efficiency was assumed for each simulation, and the Murphree efficiency equation was used to determine the vapor-phase mole fraction for component i at stage z [39,40]:

$$ME_z = \eta_z = \frac{y_z - y_{z-1}}{y_z^* - y_{z-1}} \tag{12}$$

A range of 30% to 90% stage efficiency was used to compare the range of model prediction with the experimental data. The assumption of a universal stage efficiency is based on the identical geometric properties of the commercial structured packing elements and additively manufactured

intensified device. Temperature profile and exit CO_2 concentration data were used to assess how well a stage efficiency predicted the absorption column performance for different experiments and cooling conditions.

IV. Results and Discussion

Enhancement of CO_2 capture efficiency by the additively manufactured intensified device: A series of experiments showed significant improvement in the CO_2 capture by the intensified structure packing device. The fractional percentage increase in the capture rates ranged from 4.3% to 25.1% depending on operational conditions as shown in Table 2. The feed solution temperatures were studied between 40°C and 60°C considering the broad range of practical operational conditions. The relatively short height of the absorption column (1.58 m) presented a challenge for studying the intrastage cooling effect by the intensified device using aqueous MEA because the solvent residence time was not long enough to sufficiently heat the column [27]. The height of a practical packing material in a commercial absorption column was considered to be 25–40 m [41]. For this reason, in previous work, the solvent (30 wt % aqueous MEA) was heated to 70°C prior to entering the column [27].

Table 2. Improvement in CO_2 capture efficiency by intrastage cooling using the intensified packing device. The local temperatures along the column height were measured by eight thermocouples and average measurements at the steady state were determined before and after cooling.

#	Air flow rate (LPM)	CO_2 flow rate (LPM)	CO_2 amount (%)	LAS flow rate (LPM)	CO_2 output before cooling (%)	CO_2 output after cooling (%)	Capture fractional increase (%)	Capture efficiency (%) before →after cooling	Feed temp. (°C)	Avg. temp. before cooling (n=8)	Avg. temp. after cooling (n=8)	Temperature reduction (%)	LAS condition
1	510	90	13.8	3.26	2.21	0.64	**13.5**	84.0→95.4	59	60.7 ± 3.7	52.2 ± 5.4	**14.0**	Pristine
2	510	90	14.0	3.26	1.95	0.47	**12.3**	86.0→96.6	52	59.6 ± 3.7	50.4 ± 5.4	**15.4**	Pristine
3	510	90	13.8	3.26	1.61	0.64	**8.0**	88.3→95.4	45	58.6 ± 4.8	50.1 ± 6.3	**14.5**	Pristine
4	510	90	14.7	3.26	3.18	1.57	**14.0**	78.4→89.4	41	54.5 ± 5.5	45.3 ± 6.8	**16.8**	1st regen.
5	608	107	13.1	3.26	3.75	2.23	**16.3**	71.3→82.9	44	55.2 ± 5.4	46.8 ± 7.3	**15.2**	2nd regen.
6	608	107	13.0	3.26	2.94	2.08	**8.5**	77.4→84.0	44	55.4 ± 3.6	46.9 ± 8.1	**15.3**	2nd regen.
7	425	75	13.3	3.26	1.19	0.67	**4.3**	91.1→95.0	41	52.8 ± 6.8	44.9 ± 7.5	**14.9**	3rd regen.
8	510	90	13.1	2.82	2.75	1.75	**9.7**	79.1→86.7	41	53.8 ± 5.5	46.6 ± 6.9	**13.4**	3rd regen.
9	353	62	13.3	3.26	0.79	0.44	**2.8**	94.0→96.6	41	49.8 ± 7.6	39.7 ± 8.9	**20.3**	4th regen.
10	510	90	12.8	3.65	2.16	1.13	**9.7**	83.2→91.2	41	52.7 ± 5.3	44.2 ± 7.5	**16.1**	4th regen.
11	510	90	13.1	2.39	5.85	4.71	**15.7**	55.3→64.0	41	52.3 ± 4.6	45.5 ± 7.3	**13.0**	5th regen.
12	510	90	13.0	2.82	4.92	3.25	**20.7**	62.2→75.0	41	54.2 ± 4.7	46.4 ± 6.7	**14.4**	5th regen.
13	510	90	13.2	3.26	5.74	3.86	**25.1**	56.7→70.9	41	53.5 ± 4.7	45.0 ± 7.8	**15.9**	6th regen.
14	510	90	13.1	3.26	5.33	4.73	**7.8**	59.3→63.9	41	52.1 ± 3.2	43.5 ± 8.2	**16.5**	6th regen.

*Regenerations 1 through 6 where performed by heating the solvent to 105°C for 30 min.

$$Capture\ fractional\ increase\ (\%) = \frac{Capture\ efficiency\ after\ cooling - Capture\ efficiency\ before\ cooling}{Capture\ efficiency\ before\ cooling} \times 100$$

However, we observed that the LAS during the experiments shown in Table 2 was more sensitive to temperature compared with aqueous MEA. For example, with a LAS feed temperature of 40°C, the heat generation from the CO_2-LAS absorption reaction and the corresponding heat accumulation along the column are enough to impact the CO_2 capture efficiency.

Thermal management by intrastage cooling: Time-dependent CO_2 concentration profiles before and after intrastage cooling by the intensified device were measured as shown in Figure 5a. The absorber was operated in a counter-current mode in which CO_2-lean LAS was fed to the top of the column while CO_2-rich flue gas (~14%) was fed to the bottom. As CO_2 was absorbed by the LAS, the temperature of the solvent increased as shown in Figure 5b. Initially, the CO_2 concentration rapidly dropped at the gas outlet as the entire column rapidly heated because of the amine-CO_2 absorption reaction. Column temperature measurements along the axial direction, except for the top ($T_{1,1}$), increased to 50°C or greater after 300 s. Following the observed column temperature increase, the CO_2 concentration at the gas outlet gradually increased and reached an approximate steady-state value of 1.95% for the experiment shown in Figure 5a. Subsequently, the column temperatures reached an approximate steady state (e.g., $T_{1,3}$ at 63.5°C) at 700 s of operation before cooling was introduced to the column. When water coolant at 8°C was introduced through the intensified device, the temperatures of the column rapidly decreased and reached a second steady state around 900 s. At this new steady state, the CO_2 outlet decreased from 1.95% to 0.47%, and the observed column temperatures above and below the intensified device, namely $T_{1,4}$ and $T_{1,5}$, decreased significantly from approximately 60°C to 40°C. Once sufficient time was allowed for this new steady state to be reached, the flow of solvent was stopped, while CO_2 gas concentration measurements at the exit and temperature measurements

along the column continued. The data presented in Figures 5a-e are representative of other experiments summarized in Table 2.

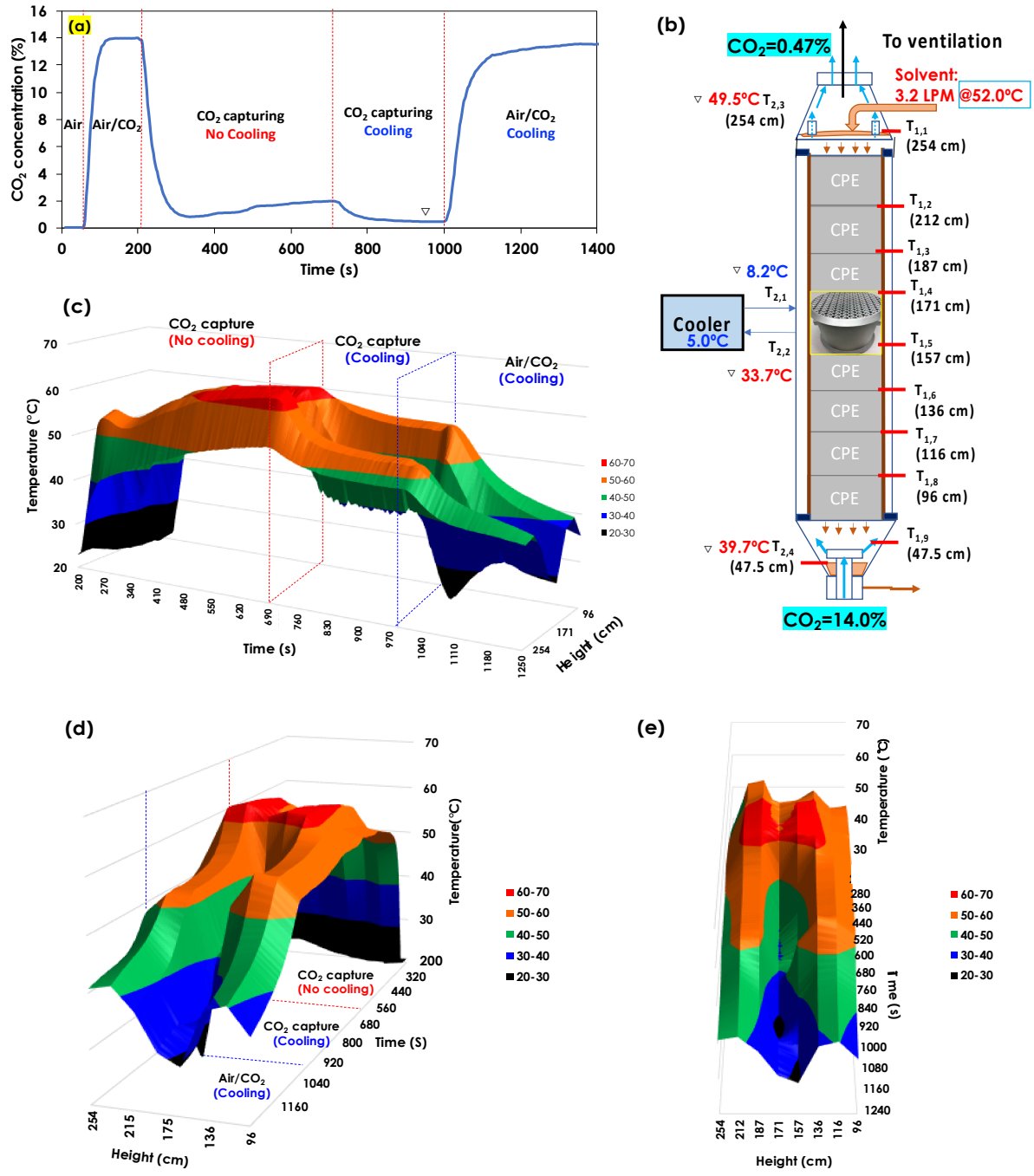

Figure 5. (a) Time-dependent CO_2 concentration profile during CO_2 absorption by the LAS with intrastage cooling. The LAS process was tested at 600 LPM gas flow rate and 14% CO_2 feed

concentration with ~50°C of the LAS feed at 3.2 LPM. (b) Schematic of column with the CO_2 concentration and temperature measurements at steady state with intrastage cooling. The reverse triangles in (a) and (b) indicate the points in time at which steady-state data for experiment 2 were recorded in Table 2. (c) Corresponding time-dependent temperature profiles along the column: front view, (d) side view, (e) top view.

Figure 6a demonstrates that the intensified device located at the middle of the column between $T_{1,4}$ and $T_{1.5}$ may supply sufficient cooling to the entire column. The temperature profiles along the column showed a bulge as a function of the gas and solvent flowrates under adiabatic conditions. The location of the temperature bulge at the onset of CO_2 absorption was observed at the upper column (Figures 5c, d, and e). This is because the CO_2-containing gas mixture was introduced in the column earlier than the solvent. The bulge location eventually moved near the middle of the column at steady state, where the intensified device was located. Like in previous work with aqueous solvent [27], when the intensified device was located near the bulge point, the heat removal rate by the device was maximized once the coolant flow was started and, at steady state, the temperature profile was in general lower than before cooling (Figures 6a and b), with two temperature bulges appearing above and below the intensified device. The temperature bulge location could be varied by the operational conditions, such as solvent and gas flow rates, solvent composition, height of packing and CO_2 concentration in the flue gas [21].

Once intrastage cooling started, a significant temperature drop was observed near the intensified device, as well as in the entire column, demonstrating effective cooling by the intensified device and an average of 9.2°C temperature reduction along the column. Figure 7 shows all axial temperature profiles and indicates that, depending on the operating conditions (e.g., feed temperature and L/G), the temperature bulge could be located at different positions before cooling. In all cases, cooling caused temperature bulges to appear above and below the intensified device. Thermal management through intrastage cooling resulted in improved CO_2

capture efficiency, decreasing the outlet flue gas CO_2 concentration and reaching a steady state of 0.47% at 950 s in Figure 6b. The corresponding capture efficiency increased from 86.0% to 96.6%, representing a fractional increase of 12.3% (Table 2).

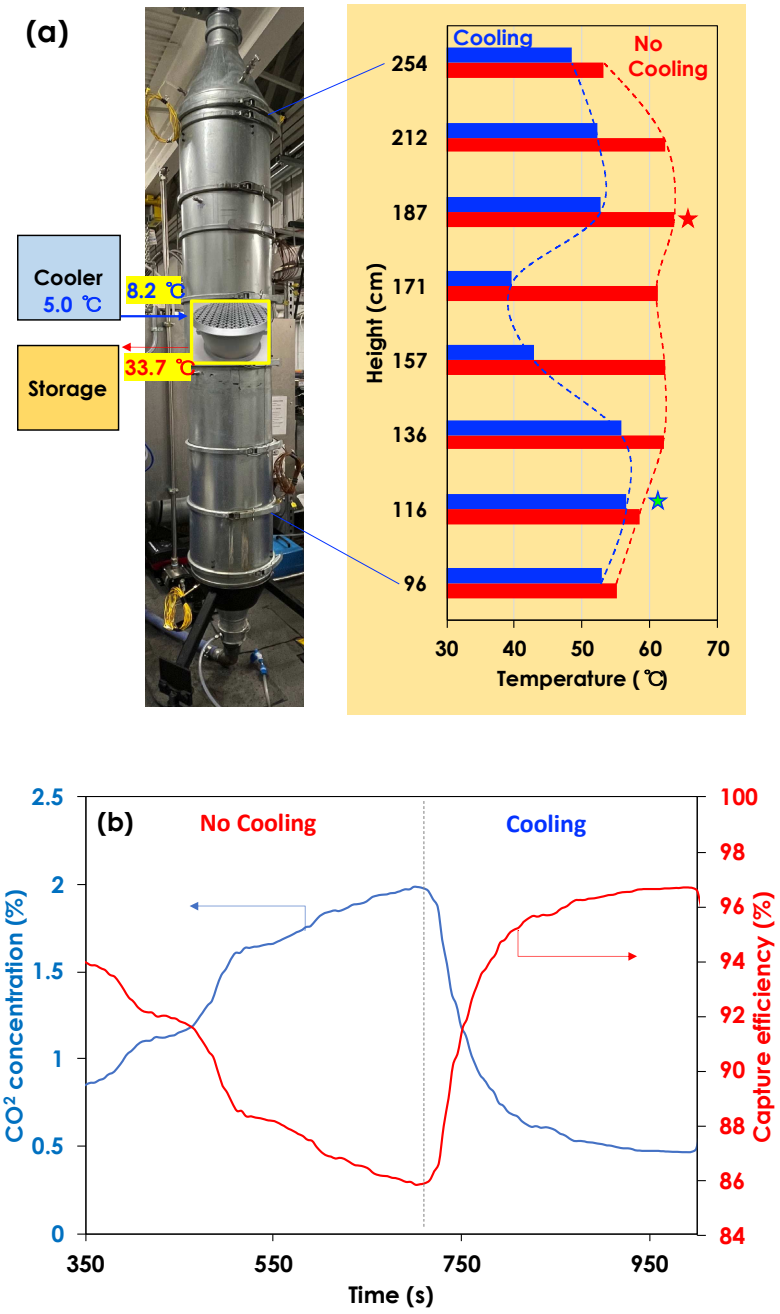

Figure 6. (a) Axial steady-state temperature profile along the column height before and after intrastage cooling. The results are from experiment 2 (in Table 2). The red and blue star signs indicate the highest temperature budge before and after cooling, respectively. (b) Time-

dependent profiles of CO_2 concentration and capture efficiency during experiment 2. The CO_2 concentration was measured at the top of the column.

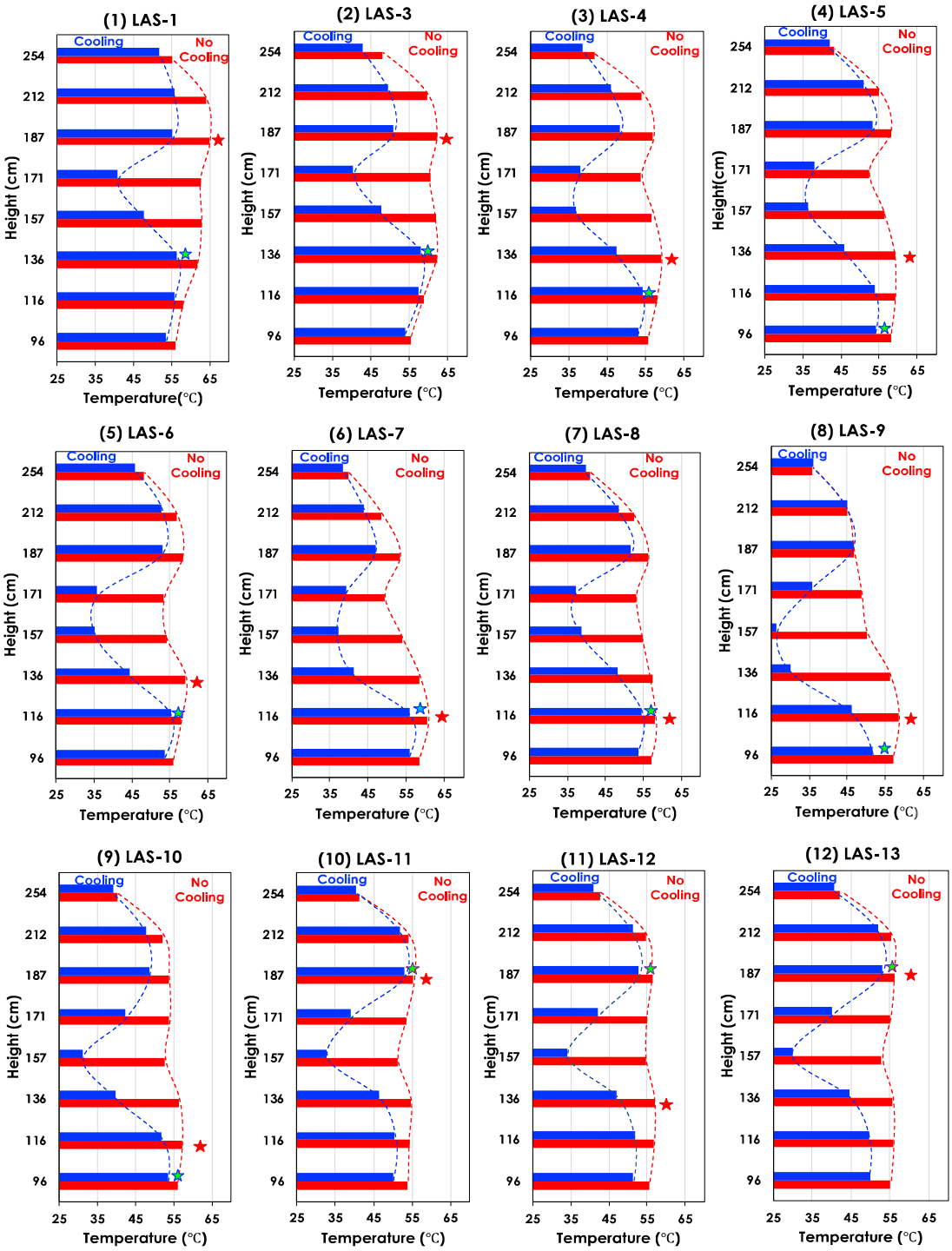

Figure 7. Axial steady-state temperature profiles along the column before and after intrastage cooling for all the experiments. Red stars and blue stars indicate the highest temperature position

along the column before and after instrastage cooling, respectively. The profile for LAS-2 is shown in Figure 6.

Effects of operating parameters on CO_2 capture enhancement: Various operating conditions were tested to evaluate the CO_2 capture improvement using the intensified device. The CO_2 outlet concentration versus inlet solvent temperature in Figure 8a suggests that the CO_2 capture efficiency by the LAS depends on the solvent temperature within the absorption column. As the solvent feed temperature decreased from 58°C to 52°C to 45°C, the CO_2 concentration at the gas exit decreased from 2.2% to 2.0% to 1.6%, respectively, at a steady state prior to cooling. After cooling, the CO_2 outflow concentrations further decreased to 0.4%–0.6%, resulting in fractional improvement in CO_2 capture efficiency of 13.5%, 12.0%, and 8.0%, respectively. The steady-state local temperature profiles for $T_{1,3}$ and $T_{1,6}$, as shown in Figure 8b, indicate that these temperatures dropped between 5°C and 12°C, a behavior correlated with the capture efficiency improvement. The position of $T_{1,3}$ and its magnitude suggest the highest heat accumulation at that point for the specific operating conditions of experiments 1–3 (Table 2). The highest fractional capture improvement occurred when the hottest axial position within the column was cooled to 55°C from 65°C. These experiments were carried out with pristine LAS, and subsequent experimental sets were tested using regenerated LAS at 105°C.

Similar to studies using aqueous MEA [24], higher ratios of liquid-to-gas (L/G) mass flow rates favor higher capture efficiency of CO_2, resulting in a trade-off between lower CO_2 outlet concentrations and increasing solvent flow rate relative to gas flow rate (Figure 8c). Intrastage cooling further improved the capture efficiency. In the experiments shown in Figures 8c and d, the liquid flow rate increased while the gas flow rate was fixed at 600 LPM (or 0.77 kg/min). A higher fractional improvement was observed at L/G=3.6, compared to that at L/G =3.1. This behavior is possibly due to nonlinearities of the system. Similar to in other experiments, the

effect of intrastage cooling shown in Figure 8d contributed to an increase in the CO_2 capture efficiency as shown in Figure 8c. Figure 8e shows that increasing the L/G ratio reduced the CO_2 outlet concentration, which is consistent with observations in Figure 8c.

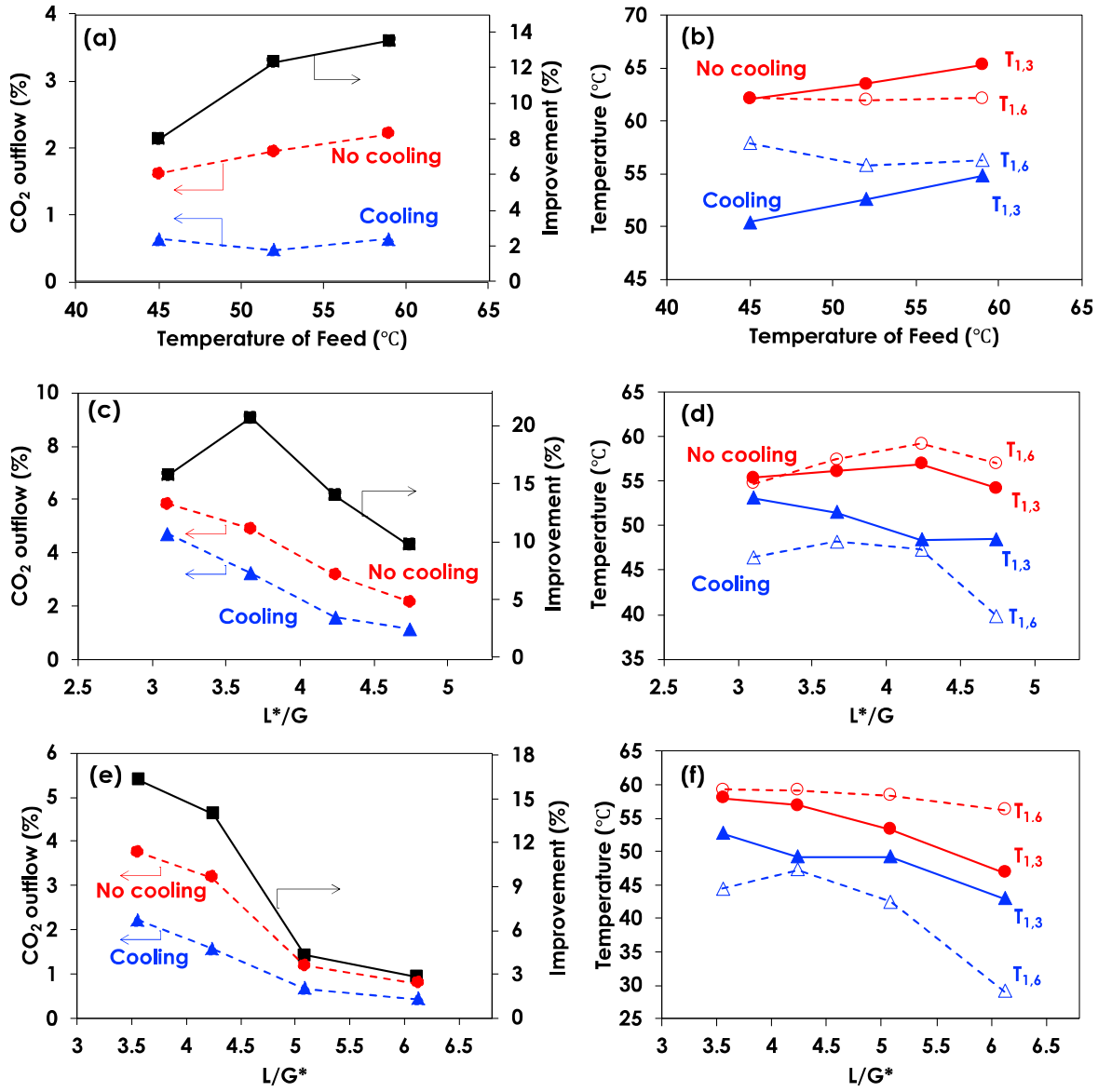

Figure 8. (a) Influence of feed temperature on CO_2 capture efficiency. The simulated flue gas concentration is 14% CO_2, and L/G=4.2. Results are from experiments 1, 2, and 3 in Table 2. (b) Corresponding local steady-state temperature profiles. (c) Influence of solvent flowrate (L*) on CO_2 capture. The flue gas flowrate (13% CO_2) was fixed at 600 LPM, and the temperature of the feed solution was at 41°C. Results are from experiments 4, 10, 11, and 12. (d) Corresponding local steady-state temperature profiles. (e) Influence of gas flowrate (G*) on CO_2 capture. The

temperature of the feed solution was 41°C and LAS flowrate was 3.26 LPM. Results are from experiments 4, 5, 7, and 9 in Table 2. (f) Corresponding local steady-state temperature profiles.

In the experiments shown in Figures 8e and f, the incoming gas flow rate decreased while the liquid flow rate remained constant at 3.26 LPM. Because of a lower incoming CO_2 mass flow rate, the overall capture efficiency increased with increasing L/G, and heat accumulation decreased as observed by changes in the column temperature profile for $T_{1,3}$ and $T_{1,6}$. The non-monotonous behavior of the temperature profile vs L/G is possibly due to nonlinearities of the system. Although the local heat accumulation was relatively small (e.g., at L/G = 6.1, experiment 9, in Figures 8e and f) at 45°C–47°C, intrastage cooling through the intensified device demonstrated an improvement of approximately 3% in the CO_2 capture efficiency by further reducing the temperature. These data suggest that the optimal temperature conditions during CO_2 absorption by the LAS may be below 45°C.

Regeneration effects on CO_2 absorption performance: A CO_2 desorption profile shown in Figure 9 was determined by heating the CO_2-rich LAS for regeneration and monitoring both the gas-phase CO_2 concentration and inorganic carbon content of the solvent. The concentration (percentage of CO_2 in gas) of the released CO_2 was determined using the CO_2 gas detector. Because of the limit of detection within 0%–32% CO_2 concentration, measurements above 85°C were not possible, but solvent measurements revealed that CO_2 desorption started at 50°C, indicating that LAS is sensitive toward temperature changes. The unique kinetic and equilibrium behavior may explain why intrastage cooling by the intensified device was effective on CO_2 absorption enhancement for this LAS formulation at intermediate feed temperatures of 40°C–60°C. For all experiments, we observed that the column was quickly heated to 50°C–60°C by the solvent before intrastage cooling was activated. At such temperatures, based on the desorption

profile shown in Figure 9, unfavorable desorption or reduced mass transfer may occur within the absorption column. The concentration profile from dissolved CO_2 concentration in the CO_2-rich LAS indicates that sufficient regeneration occurred at 105°C.

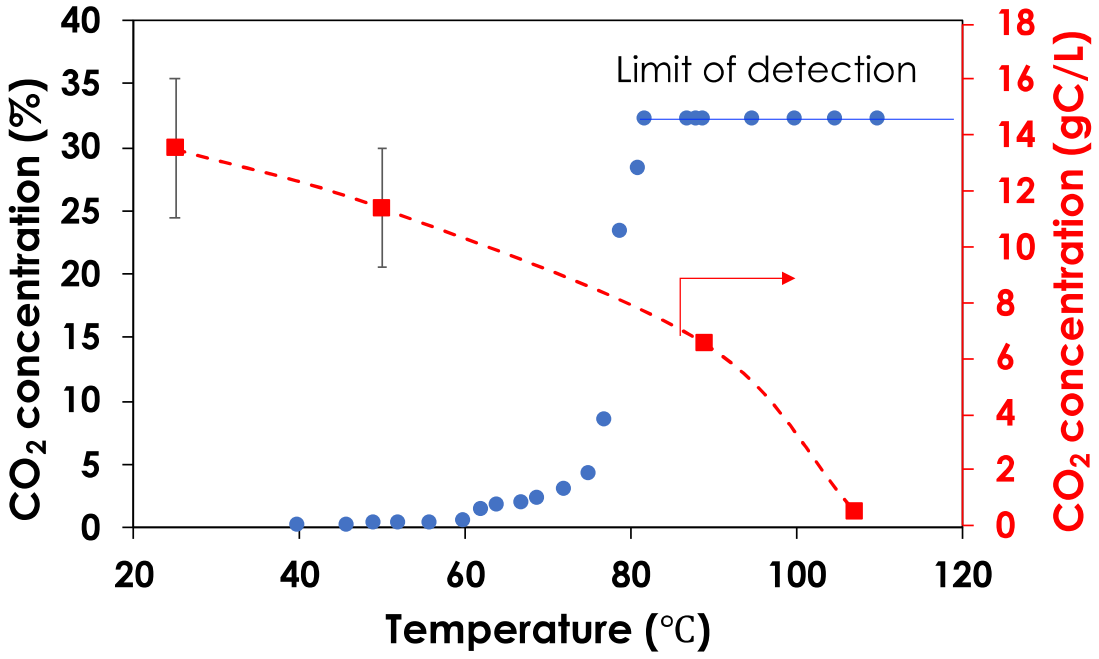

Figure 9. Influence of temperature on regeneration of CO_2-rich LAS. Blue solid circles represent CO_2 concentration (%) in evaporated gas from LAS. Red solid squares represent CO_2 concentration (gC/L) in the CO_2 rich LAS.

After repeating the regeneration process (i.e., at 105°C for 30 min), the CO_2 capture efficiency decreased as shown in Figure 10a. The regeneration profiles related to the capture efficiency were examined based on selected operating conditions, including L/G = 4.2 at a fixed liquid flow rate of 3.26 LPM and 41°C feed solvent temperature. For the 3rd and 5th regenerations, a solvent flow rate of 2.82 LPM was selected for comparison. Based on total inorganic carbon analysis and water content, as shown in Figure 10b, the composition of the regenerated CO_2-lean LAS may

have contributed to the observed decrease in CO_2 capture performance. The remaining CO_2 in the lean solvent after regeneration may have significantly affected the mass transfer driving force for CO_2 capture [36]. The steady-state temperature profiles shown in Figure 10c for the no-cooling and cooling states indicate that the accumulated heat along the column was also significantly reduced in combination with the capture efficiency reduction after the first and subsequent solvent regenerations. The lower heat accumulation implies that the rate and extent of the exothermic CO_2 gas-liquid reaction after regeneration may have decreased relative to the pristine LAS.

After six regeneration cycles, the CO_2 concentration of the lean solvent reached approximately 1 g C/L solvent, corresponding to the lowest capture efficiency for the lean solvent. In addition to the concentration of CO_2 in the lean solvent, the presence of water in the LAS may be another factor contributing to the performance of the solvent in CO_2 absorption/desorption. Previous work has reported that water in the LAS acts as an activator to increase the reaction rate with CO_2 [19]. The optimal water concentration in the LAS that keeps the solvent activated and the regeneration rate low is at 5% [19]. Addition of deionized water (5 L) to the storage tank (~95 L of the LAS) before the 3rd regeneration was used to understand the water activation effect. The water amount in the regenerated LAS, shown in Figure 10b, increased after the water addition while the remaining CO_2 amount in the lean solvent significantly decreased after the regeneration. Following this behavior, the regeneration was repeated without further addition of water to understand the efficacy of the added water for removal of CO_2 concentration in the lean solvent after multiple regenerations. The role of water may be further studied to optimize the regeneration efficiency and its effect on the CO_2 capture process with the LAS.

Table 3 shows the dissolved CO_2 and water concentrations in LAS samples before and after intrastage cooling. The dissolved CO_2 analysis in the solvent was correlated with the observed CO_2 absorption results determined by CO_2 concentration at the inlet and outlet of the gas used in the

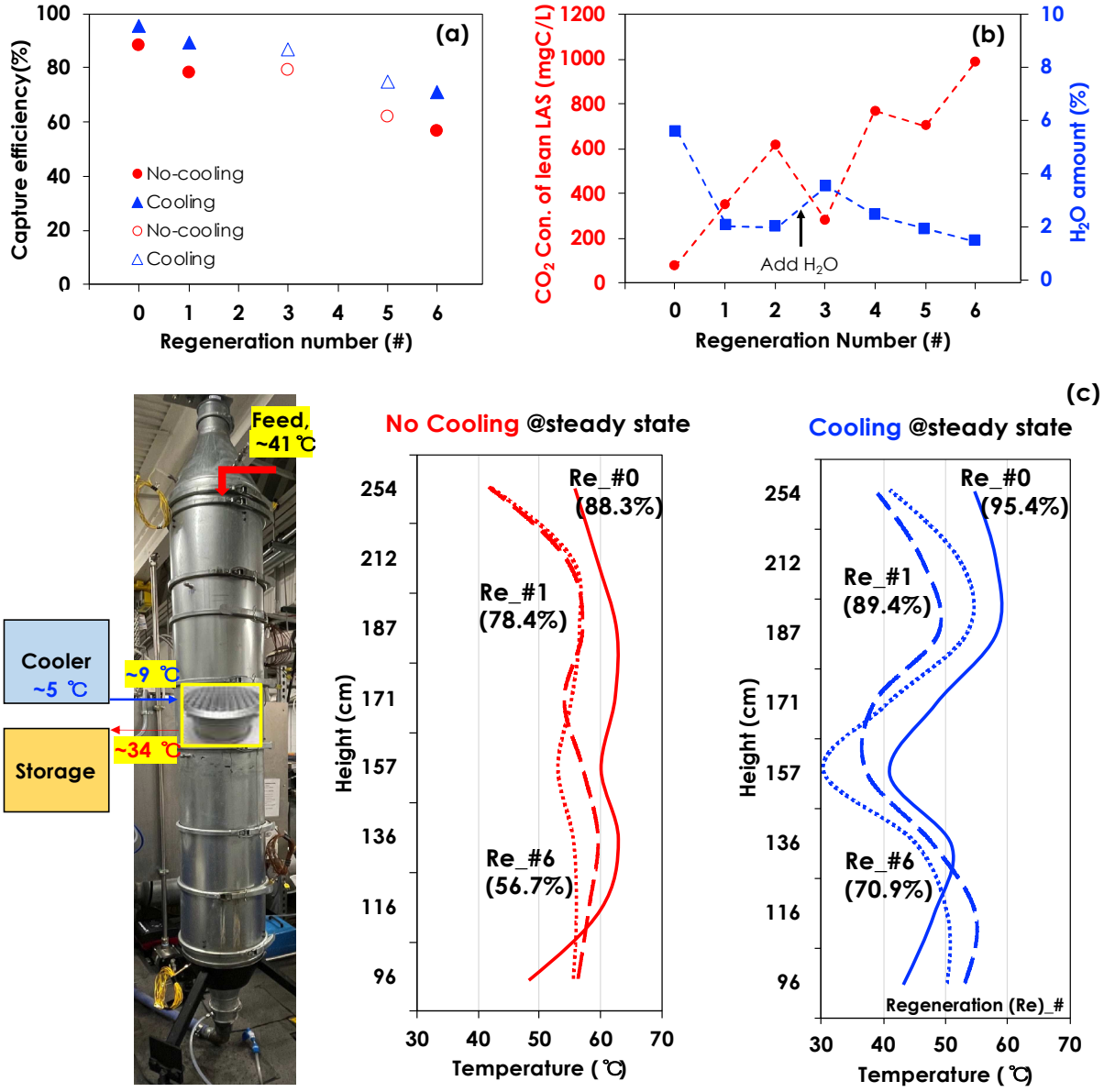

Figure 10. (a) CO_2 capture efficiency of the LAS after multiple regenerations. The solid circles indicate the results of experiments 3, 4, and 13 that were tested for pristine solvent and after

regenerations 1, and 6, whereas the empty circles indicate the results of experiments 8 and 12 after regenerations 3 and 5. (b) Corresponding CO_2 and H_2O concentrations in the CO_2 lean LAS after regeneration at 105°C for 30 min. (c) Temperature profiles of no cooling/cooling during CO_2 absorption. (Re_# stands for the regeneration number.) Re_#0: solid line (—), Re_#1: dashed line (---), Re_#6: dot line (•)

experiments. The mass balance results based on the dissolved CO_2 in the liquid solvent samples are within 2 and 40% of the gas basis for CO_2 absorption amount determined by the gas-phase measurement of CO_2. When intrastage cooling was used, there was a higher degree of absorption for CO_2 compared with adiabatic conditions in the column, and this was also correlated with the dissolved CO_2 concentrations shown in Table 3 for experiments 13 and 14. Because of changing CO_2 and water concentrations in the CO_2-lean LAS, comparing the experimental data for different regeneration cycles is difficult. The effect of water and lean CO_2 concentration may be further studied to better understand and optimize the CO_2 capture process using LAS.

Table 3. Characteristics of the LAS in CO_2 absorption and water content after capture and regeneration. The operating conditions include constant CO_2 feed rate (13%, 600 LPM) with 3.26 LAS flow rate.

Experiment		#1	#2	#3	#4	#13		#14	
Operation		Cooling	Cooling	Cooling	Cooling	No-cooling	Cooling	No-cooling	Cooling
Feed LAS	CO_2, gC/L [H_2O,%]		0.076 [5.56]		0.351 [2.01]	0.987 [1.42]		0.934 [7.59]	
Outflow LAS	CO_2, gC/L [H_2O,%]	12.89 [3.25]	11.38 [1.90]	16.28 [2.00]	8.07 [1.65]	9.50 [0.81]	9.63 [0.71]	12.98 [5.33]	13.58 [5.98]
CO_2 absorption (gCO_2/L, liquid basis)		47.0	41.4	59.4	28.9	31.2	31.7	44.2	46.4
CO_2 absorption* (gCO_2/L, gas basis)		51.3	52.0	51.3	48.1	30.4	38.09	31.9	34.4

* indicates the absorption value was determined by CO_2 gas measurement.

Heat transfer and energy analysis: The heat transfer methodology from Miramontes et al. [26,27] was used to determine the overall and individual heat transfer coefficients. The overall heat transfer coefficient may be estimated by relating the heat flux from the coolant to the log-mean temperature difference (LMTD) between the coolant and absorption column:

$$q = UA\Delta T_{lm} = m \int C_p dT \tag{13}$$

where U is the overall heat transfer coefficient, A is the contact surface area for heat exchange, ΔT_{lm} is the log-mean temperature difference, m is the mass flowrate of the coolant (water), and C_p is the heat capacity of the coolant. The integral on the right-hand side is evaluated based on the inlet and outlet temperatures for the coolant. The total contact surface area of the device, A, was reported previously by Miramontes as 2.671 m^2 [27]. The coolant-side heat transfer coefficient was calculated by assuming a constant Nusselt number of 4.36 as described in Miramontes [27,42]. The resistance in heat transfer is therefore determined by:

$$\frac{1}{U} = \frac{1}{h_c} + \frac{L}{k_{Al}} + \frac{1}{h_h} \tag{14}$$

where h_c is the coolant-side heat transfer coefficient, h_h is the absorption-side heat transfer coefficient, and L/k_{Al} is the thermal resistance of the intensified device, 6.2 x 10^{-5} K/W.

Table 4 shows the estimated overall, coolant-side and absorption-side heat transfer coefficients. Using aqueous MEA as the solvent, the absorption-side heat transfer coefficient was previously calculated between 79-148 W/m^2/K [27]. In Table 4, the absorption-side heat transfer coefficient varied between 39-111 W/m^2/K, resulting in 25-50% reduction in the heat transfer coefficient compared to aqueous MEA. The solvent here is primarily composed of an organic diluent, which would have a lower thermal conductivity compared to an aqueous based solvent. The absorption-side heat transfer coefficient can be determined by the local Nusselt number (Nu):

$$Nu = \frac{hD}{k} \tag{15}$$

where h is the heat transfer coefficient, D is the characteristic length dimension, and k is the thermal conductivity. Because h is directly proportional to the k, the thermal conductivity, the data in Table 4 suggest that the heat transfer coefficient from the absorption-side is correlated with the properties of the solvent. Previous work with aqueous MEA showed the heat transfer coefficient to be positively correlated with increasing the gas flowrate [27], but changes in the liquid flowrate were not investigated. The data here show a positive correlation with an increase in the liquid flowrate. This suggests the absorption-side Nusselt number may be related to either phases. Further study of the heat transfer properties to determine these relationships with different solvent formulations and packing configurations may help determine the dominating resistance to heat transfer for the intensified packing device.

Table 4. Estimated overall, coolant-side, and absorption-side heat transfer coefficients for experimental conditions LAS-1 through LAS-14.

	U $W/m^2/K$	h_c $W/m^2/K$	h_h $W/m^2/K$	G LPM	L LPM	Q kW	Specific Energy $MJ/kg\ CO_2$
LAS-1	67	1310	71	600	3.26	3.1	1.2
LAS-2	54	1314	56	600	3.26	3.4	1.3
LAS-3	57	1307	60	600	3.26	2.9	1.1
LAS-4	59	1300	62	600	3.26	2.6	1.0
LAS-5	70	1306	74	715	3.26	2.6	1.0
LAS-6	111	1309	122	715	3.26	2.7	1.1
LAS-7	93	1309	101	500	3.26	3.1	1.5
LAS-8	98	1308	107	600	2.82	3.0	1.4
LAS-9	50	1295	53	415	3.26	1.9	1.1
LAS-10	60	1304	63	600	3.65	2.6	1.1
LAS-11	39	1306	40	600	2.39	1.6	1.0
LAS-12	45	1310	46	600	2.82	1.9	1.0
LAS-13	42	1296	44	600	3.26	2.0	1.1
LAS-14	50	1294	52	600	3.26	1.8	1.1

The intrastage cooling energy requirement may be estimated by the temperature difference of the inlet and outlet of the coolant. As the LAS-CO_2 system has shown a high degree of sensitivity for cooling to improve the CO_2 capture, the energy for intrastage cooling should be considered as part of the overall energy balance of a LAS CO_2 capture process. In Table 4, the energy, Q, used to estimate the heat transfer coefficients is shown to vary between 1.6-3.4 kW. This energy may be converted to a specific energy based on the CO_2 captured in the column by the following relationship:

$$q = \frac{Q}{m_{CO_2,r}} \tag{16}$$

where q is the specific energy for intrastage cooling, Q is the coolant energy utilized in the experiment, defined by Eq. 13, and $m_{CO_2,r}$ is the CO_2 removed in the absorption column with cooling. This specific energy may be considered as part of an overall energy requirement for a CO_2 capture plant that utilizes LAS as the solvent. As shown in Table 4, the specific energy for the LAS-CO_2 system cooling varies between 1.0-1.5 MJ /kg CO_2 captured. For more hydrophobic water-lean solvents, such as LAS, the estimated reboiler specific energy is estimated to be around 1.5-2.5 MJ/kg CO_2 [15]. Combining these values suggests that the specific energy may be comparable to an aqueous solvent system. Therefore, a more comprehensive energy analysis should be considered in future work that considers the effect of adiabatic versus cooling conditions of these solvents and how heat integration of a CO_2 capture plant may improve the energy balance for a LAS-CO_2 system compared with aqueous solvents.

CO_2 solubility and equilibrium-stage modeling: Two modeling approaches may be used for estimating the absorber performance for removal of CO_2: equilibrium-based models and rate-based models. Rate-based models have shown accurate prediction of the behavior for aqueous

amine solvents for flue gas carbon capture absorption conditions given that mass transfer from the flue gas to the solvent can depend on reaction within the liquid phase [39,43,44]. To properly account for rate-based modeling methods, the reaction kinetics between CO_2 and the amine solvent, the mass transfer between gas and liquid phases, and the vapor-liquid equilibria must be described accurately [45]. Therefore, these modeling approaches may be computationally intensive or require commercial process simulation software as well as detailed physical and transport properties for the solvent. Equilibrium-based models assume liquid and vapor leaving a stage within a packed column are in equilibrium with each phase, and this assumption includes chemical, thermal, and mechanical equilibria [43,44]. Only the CO_2 solubility and physical properties of the solvent are needed to estimate the absorption using an equilibrium-based modeling approach, reducing the complexity of the simulations. However, this approach may not necessarily be used a priori to design a new absorption column or transfer models to different operational scales, but these simulation tools may be useful in understanding the observed experimental behavior of a given solvent for removing CO_2 from flue gas.

To further simplify the equilibrium-based model, a semi-empirical solubility model for the LAS-CO_2 system was used based on a previously published semi-empirical model from Chen and Rochelle [36]. The model may be used to describe equilibria of CO_2 between flue gas and LAS in an absorption column, but this model cannot describe changes in CO_2 solubility with variations in the solvent formulation. Figure 11 shows the parity plot demonstrating how well this model describes the prediction of the equilibrium CO_2 partial pressure. Although there is generally good prediction of the equilibrium partial pressure below 1 bar for the entire temperature range, there is considerable deviation at the higher partial pressures, which are not relevant for the absorber conditions considered in CO_2 capture experiments. Further work to

develop vapor-liquid equilibrium (VLE) models, such as electrolyte-NRTL or Pitzer activity-based models, may provide more accuracy and account for changes in the composition of the main constituents of the solvent [46,47,48].

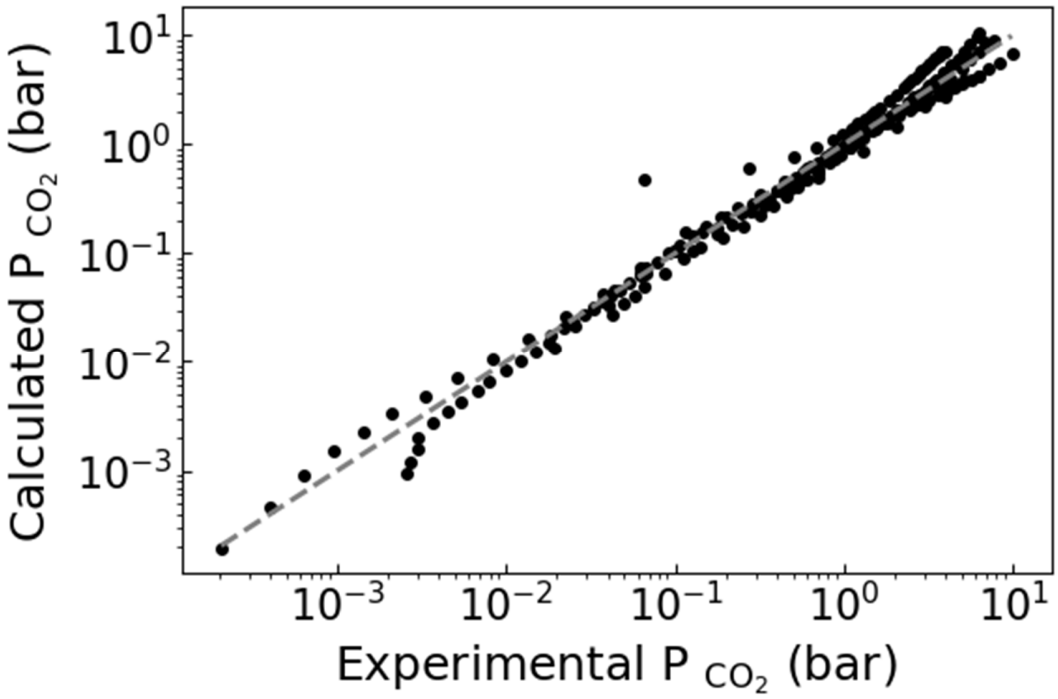

Figure 11. Parity plot of experimental CO_2 equilibrium partial pressure with calculated partial pressure from the Virial model.

Following the simulation methodology described previously, simulations of absorption experiments were performed to compare predictions of the equilibrium-based absorption model with experiments before and after intrastage cooling. Equilibrium-based simulations of experiments 1–3 were performed based on experimental conditions from Table 2. These experiments used the pristine LAS and would be best described by the solubility model above because no regeneration had been applied to the solvent. Given the pristine solvent used in these experiments, the lean CO_2 loading was assumed negligible in simulations. All simulations were performed using an algorithm developed in Python, and physical property data, such as heat

capacity, heat of vaporization, and heat of formation, were obtained from Design Institute for Physical Properties (DIPPR) or Aspen Properties [49]. Figure 12 shows the temperature profile and the predicted CO_2 profile compared with the measured temperatures and the inlet and outlet CO_2 concentrations for experiment 1 before and after cooling. Prior to cooling, the simulations under assumption of adiabatic conditions showed good agreement between the measured temperature profile and simulations that assume a stage efficiency of 60% or greater. However, the CO_2 removal predicted by the simulations under adiabatic conditions (Figure 12a) did not adequately match the experimental data at lower stage efficiencies despite the agreement with the temperature profile (Figure 12c). Only at a stage efficiency of 90% or greater did the simulation and experiment show agreement for the CO_2 outlet concentration. This was also observed in simulations of experiments 2 and 3. The stage efficiency in these simulations served as an empirical means to account for effects of mass and heat transfer and reaction kinetics that can alter the absorption behavior [43,50]. The high stage efficiency necessary to predict both an accurate temperature profile and CO_2 outlet concentration under adiabatic conditions suggests the solvent may not show the same rate-based limitations as aqueous amine solvents.

With intrastage cooling applied within the device, there is an increase in the amount of CO_2 removed by the solvent compared with adiabatic conditions shown by both the experiments and simulations. In Figure 12b, the CO_2 profiles from the simulations between a stage efficiency of 60% and 90% agree with the observed CO_2 outlet concentration in the experiment. The temperature profiles shown in Figure 12d suggest that at higher stage efficiency (where more mass transfer of CO_2 from the gas phase to the liquid phase occurs), the cooling in the additively manufactured device had less of an effect on the stage temperature, possibly because of the increased heat generated by CO_2 absorption. Stages before and after cooling showed agreement

between experimentally observed temperature profile and simulations between 60% and 90% stage efficiency. Because the heat removed by cooling was calculated based on the measured temperature of the coolant entering and leaving the packing, there is a limited degree of temperature reduction at these higher stage efficiencies.

Based on literature [21] and modeling results (see Figure 12c), a temperature bulge may be located anywhere in the column depending on the L/G ratio. Due to the short column height (1.58m), a single intrastage cooling element is enough to control the temperature increase in the entire column, resulting in enhanced CO_2 capture efficiency. However, our preliminary calculations suggest that a longer column (>4 m) would need more intrastage cooling elements. The location of those elements would again depend on the L/G ratio for optimal performance. Further simulation work to understand the individual enthalpic effects, such as heat of absorption or heat of vaporization, on the calculated temperature profile under adiabatic and cooling conditions may provide improved understanding on the CO_2 capture process using simulations. This would require more experimental data to better estimate the effect of solvent composition on the vapor-liquid equilibria as well as other thermodynamic properties of the solvent.

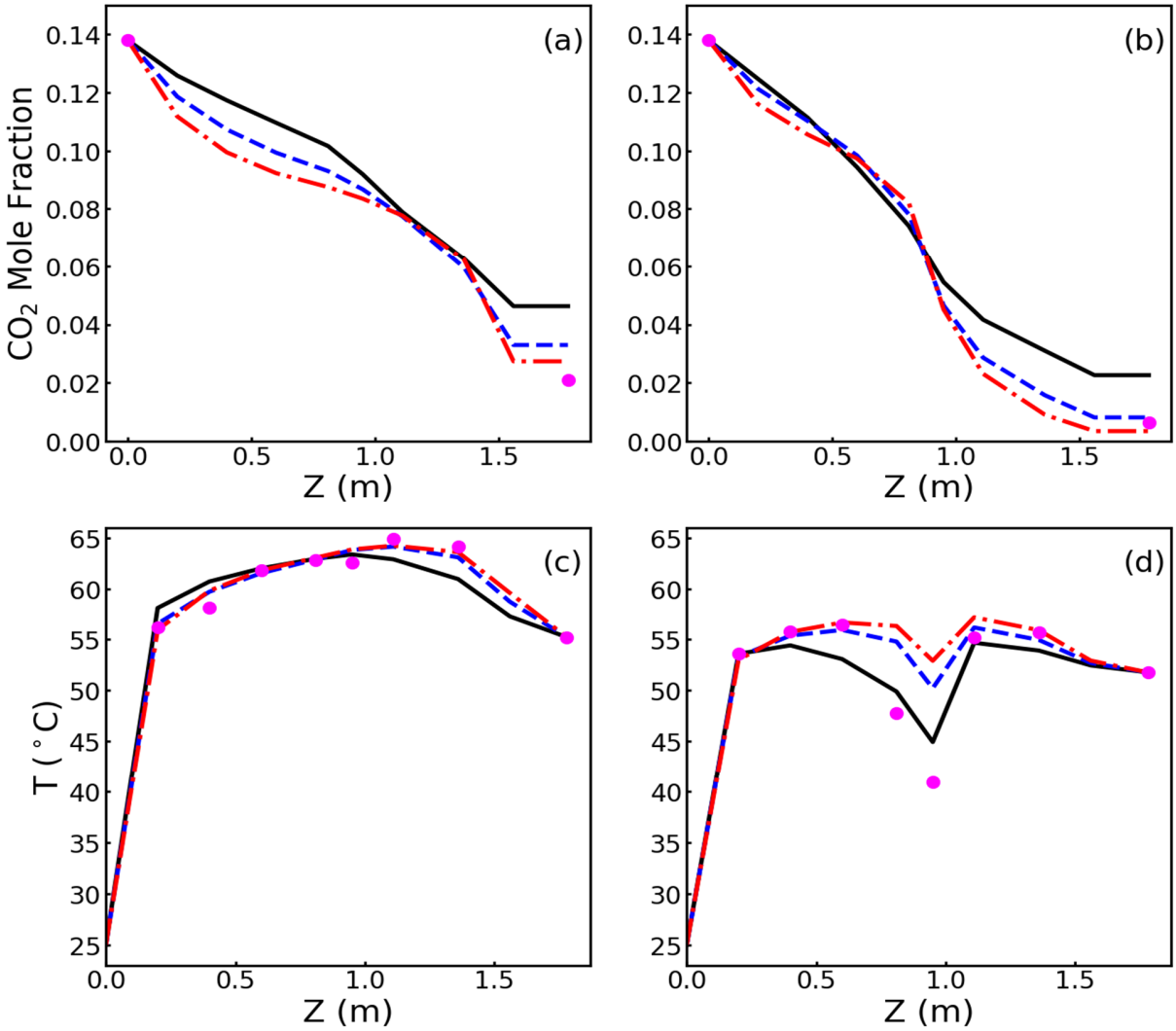

Figure 12. CO_2 concentration profiles along the absorption column (a) before and (b) after cooling; and temperature profiles along the absorption column (c) before and (d) after cooling. Symbols are from experiment 1, and lines are from different simulations varying the stage efficiency at 30% (black, solid), 60% (blue, dashed), and 90% (red, dash-dot).

V. Conclusions

Highly efficient CO_2 capture using an LAS and intrastage cooling has been demonstrated using an additively manufactured intensified packing device. The LAS was found to be a thermally sensitive solvent because of the lower heat capacity of the organic diluent compared with that of water, as well as the intrinsic thermodynamic behavior of the solvent. Based on a theoretical

model, the highly efficient thermal management and its mass transfer enhancement were demonstrated using intrastage cooling by the intensified packing device. A 15% temperature reduction and a fractional CO_2 capture enhancement of up to 25% were achieved. The performance of the LAS with respect to CO_2 capture was systematically investigated, and effects of solvent feed temperature, L/G mass flow rate ratio, and solvent regeneration were studied. Future work may be focused on better understanding the regeneration effects and long-term performance of the LAS with the goal to optimize the regeneration conditions and to balance the water content as an effective activator and as a diluent. The energy requirements for intrastage cooling versus regeneration should also be considered in comparison with commercial aqueous solvents. Additional work may also focus on optimizing the design of the intensified devices to be more effective and reducing the length of column for a compact design for lower-concentration CO_2 gases, such as flue gas generated from natural gas combustion.

Acknowledgments

This research was funded by the Office of Fossil Energy of the US Department of Energy. Technical help by Mr. Scott Palko of the Applied Catalysis and Emissions Research Group of Oak Ridge National Laboratory is gratefully acknowledged. The authors are also thankful to Drs. Marty Lail and Paul Mobley of RTI International for providing the low-aqueous solvent for this study and also for helpful discussions. The authors are also thankful to Ms. Olivia Shafer for editing the manuscript.

References

[1] D. Feng, J. Gao, Y. Zhang, H. Li, Q. Du, S. Wu, Mass transfer in ammonia-based CO_2 absorption in bubbling reactor under static magnetic field, Chem. Eng. J. 338 (2018) 450–456.

[2] M.A. Naeem, A. Armutlulu, Q. Imtiaz, F. Donat, R. Schäublin, A. Kierzkowska, C.R. Müller, Optimization of the structural characteristics of CaO and its effective stabilization yield high-capacity CO_2 sorbents, Nat. Commun. 9 (2018) 2408.

[3] K. Kumar, C.N. Dasgupta, B. Nayak, P. Lindblad, D. Das, Development of suitable photobioreactors for CO_2 sequestration addressing global warming using green algae and cyanobacteria, Bioresour. Technol. 102 (2011) 4945–4953.

[4] R. Khalilpour, K. Mumford, H. Zhai, A. Abbas, G. Stevens, E.S. Rubin, Membrane-based carbon capture from flue gas: A review, J. Clean. Prod. 103 (2015) 286–300.

[5] F. Chu, S. Li, H. Chen, L. Yang, O. Ola, M. Maroto-Valer, X. Du, Y. Yang, Modeling photocatalytic conversion of carbon dioxide in bubbling twin reactor, Energy Convers. Manage. 149 (2017) 514–525.

[6] P. Linga, R. Kumar, P. Englezos, Gas hydrate formation from hydrogen/carbon dioxide and nitrogen/carbon dioxide gas mixtures, Chem. Eng. Sci. 62 (2007) 4268–4276.

[7] D. Aaron, C. Tsouris, Separation of CO_2 from flue gas: A Review, Sep. Sci. Tech., 40 (2005) 321–348.

[8] J. Oexmann, A. Kather, Minimising the regeneration heat duty of post-combustion CO_2 capture by wet chemical absorption: The misguided focus on low heat of absorption solvents, Int. J. Greenh. Gas Control 4 (2010) 36–43.

[9] R. Idem, M. Wilson, P. Tontiwachwuthikul, A. Chakma, A. Veawab, A. Aroonwilas, D. Gelowitz, Pilot plant studies of the CO_2 capture performance of aqueous MEA and mixed MEA/MDEA solvents at the University of Regina CO_2 capture technology development plant and the boundary dam CO_2 capture demonstration plant, Ind. Eng. Chem. Res. 45 (2006) 2414–20.

[10] R. Notz, H.P. Mangalapally, H. Hasse, Post combustion CO_2 capture by reactive absorption: Pilot plant description and results of systematic studies with MEA, Int. J. Greenh. Gas Control 6 (2012) 84–112.

[11] K. Li, A. Cousins, H. Yu, P. Feron, M. Tade, W. Luo, J. Chen, Systematic study of aqueous monoethanolamine-based CO_2 capture process: Model development and process improvement, Energy Sci. Eng. 4 (2016) 23–39.

[12] A. Schäffer, K. Brechtel, G. Scheffknecht, Comparative study on differently concentrated aqueous solutions of MEA and TETA for CO_2 capture from flue gases, Fuel 101 (2012) 148–153.

[13] Y. Jiang, Z. Zhang, J. Fan, J. Yu, D. Bi, B. Li, Z. Zhao, M. Jia, A. Mu, Experimental study on comprehensive carbon capture performance of TETA- based nanofluids with surfactants, Int. J. Greenh. Gas Control 88 (2019) 311–320.

[14] R.F. Zheng, D. Barpaga, P.M. Mathias, D. Malhotra, P. K Koech, Y. Jiang, M. Bhakta, M. Lail, A.V. Rayer, G.A. Whyatt, C.J. Freeman, A.J. Zwoster, K.K. Weitz, D.J. Heldebrant, A single-component water-lean post-combustion CO_2 capture solvent with exceptionally low operational heat and total costs of capture – Comprehensive experimental and theoretical evaluation, Energy Environ. Sci. 13 (2020) 4106–4113.

[15] M. Lail, J. Tanthana, L. Coleman, Non-aqueous solvent (NAS) CO_2 capture process, Energy Proc. 63 (2014) 580–594.

[16] W. Conway, Q. Yang, S. James, C. Wei, M. Bown, P. Feron, G. Puxty. Designer amines for post combustion CO_2 capture processes, Energy Proc. 63 (2014) 1827–1834.

[17] J. Oexmann, C. Hensel, A. Kather, Post-combustion CO_2-capture from coal-fired power plants: preliminary evaluation of an integrated chemical absorption process with piperazine-promoted potassium carbonate. Int. J. Greenh. Gas Control 2 (2008) 539–552.

[18] A. Chakma, CO_2 capture processes—Opportunities for improved energy efficiencies, Energy Convers. Manage. 38 (1997) S51–S56.

[19] A.V. Rayer, P.D. Mobley, M. Soukri, T.R. Gohndrone, J. Tanthana, J. Zhou, M. Lail, Absorption rates of carbon dioxide in amines in hydrophilic and hydrophobic solvents, Chem. Eng. J. 348 (2018) 514–525.

[20] B. Han, C. Zhou, J. Wu, D. J. Tempel, H. Cheng. Understanding CO_2 capture mechanisms in aqueous Monoethanolamine via first principles simulations, J. Phys. Chem. Lett. 2 (2011) 522–526.

[21] H.M. Kvamsdal, G.T. Rochelle, Effects of the temperature bulge in CO_2 absorption from flue gas by aqueous monoethanolamine, Ind. Eng. Chem. Res. 47 (2008) 867–875.

[22] J.M. Plaza, D.V. Wagener, G.T. Rochelle, Modeling CO_2 capture with aqueous monoethanolamine, Int. J. Greenh. Gas Control Energy 4 (2010) 161–166.

[23] P. Galindo, A. Schäffer, K. Brechtel, S. Unterberger, G. Scheffknecht, Experimental research on the performance of CO_2-loaded solutions of MEA and DEA at regeneration conditions. Fuel 101 (2012) 2–8.

[24] J.C. Morgan, A.S. Chinen, B. Omell, D. Bhattacharyya, C. Tong, D.C. Miller, B. Buschle, M. Lucquiaud, Development of a rigorous modeling framework for solvent-based CO_2 capture.

Part 2: Steady-state validation and uncertainty quantification with pilot plant data, Ind. Eng. Chem. Res. 57 (2018) 10464–10481.

[25] S. Bolton, A. Kasturi, S. Palko, C. Lai, L. Love, J. Parks, X. Sun, C. Tsouris, 3D printed structures for optimized carbon capture technology in packed bed columns, Sep. Sci. Tech. 54 (2019) 2047–2058.

[26] E. Miramontes, L. Love, C. Lai, X. Sun, C. Tsouris, Additively manufactured packed bed device for process intensification of CO_2 Absorption and other chemical processes, Chem. Eng. J. 388 (2020) 124092.

[27] E. Miramontes, E. A. Jiang, L.J. Love, C. Lai, X. Sun, C. Tsouris. Process intensification of CO_2 absorption using a 3D printed intensified packing device, AIChE J. 66 (2020) e16285.

[28] Y. Kim, L. K. Park, S. Yiacoumi, C. Tsouris. Modular chemical process intensification: a review. Ann Rev Chem Biomol Eng. 8 (2017) 359- 380.

[29] Z. Anxionnaz, M. Cabassud, C. Gourdon, P. Tochon, Heat exchanger/reactors (HEX reactors): concepts, technologies: state-of- the-art. Chem Eng Process. 47 (2008) 2029-2050.

[30] M. S. Jassim, G. Rochelle, D. Eimer, C. Ramshaw, Carbon dioxide absorption and desorption in aqueous Monoethanolamine solutions in a rotating packed bed. Ind. Eng. Chem. Res. 46 (2007) 2823–2833.

[31] C. Xie, Y. Dong, L. Zhang, G. Chu, Y. Luo, B. Sun, X. Zeng, J. Chen, Low-concentration CO_2 capture from natural gas power plants using a rotating packed bed reactor. Energy Fuel. 33 (2019) 1713–1721

[32] J. M. MacInnes, A.A. Ayash, G.R.M. Dowson, CO_2 absorption using diethanolamine-water solutions in a rotating spiral contactor. Chem. Eng. J. 307 (2017) 1084–1091.

[33] H. Ganapathy, S. Steinmayer, A. Shooshtari, S. Dessiatoun, M. M. Ohadi, M. Alshehhi, Process intensification characteristics of a microreactor absorber for enhanced CO_2 capture. Appl Energy. 162 (2016) 416–427.

[34] T.C. Merkel, H. Lin, X. Wei, R. Baker, Power plant post-combustion carbon dioxide capture: an opportunity for membranes. J. Membr. Sci. 359 (2010) 126–139.

[35] R.P. Lively, R.R. Chance, W.J. Koros, Enabling Low-cost CO_2 capture via heat integration. Ind. Eng. Chem. Res. 49 (2010) 7550–7562.

[36] X. Chen, G.T. Rochelle, Aqueous piperazine derivatives for CO_2 capture: Accurate screening by a wetted wall column, Chem. Eng. Res. Des. 89 (2011) 1693–1710.

[37] M. Gupta, E.F. Silva, A. Hartono, H.F. Svendsen, Theoretical study of differential enthalpy of absorption of CO_2 with MEA and MDEA as a function of temperature, J. Phys. Chem. B 117 (2013) 9457–9468.

[38] T.J. Edwards, G. Maurer, J. Newman, J. M. Prausnitz, Vapor-liquid equilibria in multicomponent aqueous solutions of volatile weak electrolytes. AIChE J. 24 (1978) 966-976.

[39] P. Mores, N. Scenna, S. Mussati, Post-combustion CO_2 capture process: Equilibrium stage mathematical model of the chemical absorption of CO_2 into monoethanolamine (MEA) aqueous solution, Chem. Eng. Res. Des. 89 (2011) 1587–1599.

[40] P. Mores, N. Scenna, S. Mussati, A rate based model of a packed column for CO_2 absorption using aqueous monoethanolamine solution, Int. J. Greenh. Gas Control 6 (2012) 21–36.

[41] P. Broutin, P. Briot, S. Ehlers, A. Kather, Benchmarking of the DMX^{TM} CO_2 capture process, Energy Procedia 114 (2017) 2561–2572.

[42] F.P. Incropera, D.P. Dewitt, Fundamentals of Heat and Mass Transfer. 7th ed. Chichester: John Wiley and Sons; 2011.

[43] M. Afkhamipour, M. Mofarahi, Comparison of rate-based and equilibrium-stage models of a packed column for post-combustion CO_2 capture using 2-amino-2-methyl-1-propanol (AMP) solution, Int. J. Greenh. Gas Control 15 (2013) 186–199.

[44] M. Amirkhosrow, J.-F. Pérez-Calvo, M. Gazzani, M. Mazzotti, E. Nemati Lay, Rigorous rate-based model for CO_2 capture via monoethanolamine-based solutions: effect of kinetic models, mass transfer, and holdup correlations on prediction accuracy, Sep. Sci. Technol. (2020) 1–19.

[45] R. Baur, A.P. Higler, R. Taylor, R. Krishna, Comparison of equilibrium stage and nonequilibrium stage models for reactive distillation, Chem. Eng. J. 76 (2000) 33–47.

[46] D.M. Austgen, G.T. Rochelle, X. Peng, C.C. Chen, Model of vapor liquid equilibria for aqueous acid gas-alkanolamine systems using the electrolyte-NRTL equation, Ind. Eng. Chem. Res. 28 (1989) 1060–1073.

[47] T. Nakagaki, H. Isogai, H. Sato, J. Arakawa, Updated e-NRTL model for high-concentration MEA aqueous solution by regressing thermodynamic experimental data at high temperatures, Int. J. Greenh. Gas Control 82 (2019) 117–126.

[48] M. Wagner, I. von Harbou, J. Kim, I. Ermatchkova, G. Maurer, H. Hasse, Solubility of carbon dioxide in aqueous solutions of monoethanolamine in the low and high gas loading regions, J. Chem. Eng. Data 58 (2013) 883–895.

[49] American Institute of Chemical Engineers, Design Institute for Physical Properties, DIPPR Project 801 - Full Version, Design Institute for Physical Property Research/AIChE.

[50] M. Duss, R. Taylor, Predict distillation tray efficiency, Chem. Eng. Prog. (2018) 24–30.